PRAMANA — journal of physics

Vol. 82, No. 3
March 2014
pp. 515–527

Impact of density-dependent symmetry energy and Coulomb interactions on the evolution of intermediate mass fragments

KARAN SINGH VINAYAK and SUNEEL KUMAR*
School of Physics and Material Science, Thapar University, Patiala 147 004, India
*Corresponding author. E-mail: suneel.kumar@thapar.edu

MS received 27 May 2013; revised 7 October 2013; accepted 25 November 2013
DOI: 10.1007/s12043-014-0716-7; ***e*Publication:** 7 March 2014

Abstract. Within the framework of isospin-dependent quantum molecular dynamics (IQMD) model, we demonstrate the evolution of intermediate mass fragments in heavy-ion collisions. In this paper, we study the time evolution, impact parameter, and excitation energy dependence of IMF production for the different forms of density-dependent symmetry energy. The IMF production and charge distribution show a minor but considerable sensitivity towards various forms of density-dependent symmetry energy. The Coulomb interactions affect the IMF production significantly at peripheral collisions. The IMF production increases with the stiffness of symmetry energy.

Keywords. Symmetry energy; isospin-dependent quantum molecular dynamics; intermediate mass fragments; Coulomb interactions.

PACS Nos 25.70.Pq; 25.70.–z; 24.10.Lx.

1. Introduction

It is worth mentioning that the heavy-ion reactions from low to relativistic energies has the ability to mark the behaviour of highly dense and thermalized nuclear matter formed during the collision (i.e., nuclear equation of state). The compressed nucleus undergoes a phase transition which leads to the fragmentation of highly thermalized nuclear matter. The shattering of the target and projectile into large number of fragments after the collision is a complex phenomenon. The size and multiplicity of the fragments scale with the incident energy, colliding geometry, and size of the colliding partners. At low incident energies, Pauli principle dominates and blocks any significant scattering of the nucleons [1,2], which suppress the production of free nucleons (FNs) ($A = 1$) and light mass fragments (LMFs) ($2 \leq A \leq 4$) and enhance the production of intermediate mass fragments (IMFs) ($5 \leq A \leq A_{\text{tot}}/6$) and heavy mass fragments (HMFs) ($5 \leq A \leq A_{\text{tot}}/3$). However, larger incident energies result in more violent collision producing a large number of

lighter fragments (FN and LMF). In heavy-ion collisions, high densities are achievable for a short time span. The study of fragmentation can give us a glimpse of nuclear matter in the events of big bang, supernova explosions, and in the interior of neutron stars. Therefore, it becomes possible to understand the thermodynamical properties of strongly interacting matter.

In addition to the reaction conditions, the symmetry energy, i.e. the isospin-dependent part of nuclear equation of state, affect the dynamics of heavy-ion reactions drastically. An in-depth knowledge of the symmetry energy, and its variation with the density, is not only essential for the nuclear physics but also has a crucial role in determining the structure and composition of neutron stars [3,4]. The density dependence of the symmetry energy can be parametrized as $E_{\rm symm}(\rho) = E_{\rm symm}(\rho_0)(\rho/\rho_0)^{\gamma}$ [5–9], where the value of γ describes the stiffness (or strength) of the symmetry energy.

The fragment production in heavy-ion collisions has been of great physical importance in order to study the reaction dynamics at low densities. The study of nuclear symmetry energy, the neutron skin thickness and the percentage of energy-weighted sum rule exhausted by the pygmy dipole resonance in ^{68}Ni+^{132}Sn, are useful for the investigation of neutron radii and the observables which can shed light on the density dependence of symmetry energy [10,11]. The collective flow [9], pygmy dipole resonance, and neutron skin thickness [4,11] are suggested to analyse the behaviour and strength of symmetry energy at supradensities. Some constraints on the density dependence of symmetry energy are available at the low density region but the situation becomes very much uncertain at high densities. Shetty and Yennello [12] provided an experimental overview of the symmetry energy, which described the various attempts made to understand the behaviour of symmetry energy at densities above and below the normal nuclear density. Also, it was concluded that experimentally, the symmetry energy is not a directly measurable quantity and has to be extracted from observables associated with the symmetry energy [12].

The aim of the present study is to analyse the IMF production for various forms of density dependence of the symmetry energy, which can be useful to track the role of symmetry energy at densities less than the normal nuclear matter density ($\rho < \rho_0$). We here plan to investigate the impact parameter and excitation energy dependence of the IMF production subjected to different parametrizations of the density dependence of symmetry energy. In addition to that, we study the effect of Coulomb interactions on the fragment formation. The charge distribution of nuclear matter in heavy-ion collisions is analysed and the theoretical predictions have been compared with experimental data.

The present work has been carried out within the framework of isospin-dependent quantum molecular dynamics (IQMD) model [13]. This article is organized as follows. We discuss the model briefly in §2. Our results are presented in §3, and we summarize the results in §4.

2. Isospin-dependent quantum molecular dynamics (IQMD) model

The IQMD model [13] which is the extension of QMD model [14] is based on the molecular dynamics picture, where nucleons interact via two- and three-body mutual interactions. Careful analysis by Aichelin and co-workers proved that these models carry essential physics and can explain the phenomena of collective flow [15–17], multifragmentation

[18–21], particle production [22,23], isospin dynamics [24–27] etc. As of now, it is clear that the relativistic effects do not play a role in the energy range of the present analysis [28,29].

In IQMD model, the nucleons of the target and the projectile interact via two- and three-body Skyrme forces, Yukawa potential, and Coulomb interactions. In addition to the use of explicit charge states of all baryons and mesons, a symmetry potential between protons and neutrons corresponding to the Bethe–Weizsacker mass formula has been included. The hadron propagation is governed by the classical Hamilton equations of motion:

$$\frac{\mathrm{d}\vec{r}_i}{\mathrm{d}t} = \frac{\mathrm{d}\langle H\rangle}{\mathrm{d}\,p_i}; \qquad \frac{\mathrm{d}\vec{p}_i}{\mathrm{d}t} = -\frac{\mathrm{d}\langle H\rangle}{\mathrm{d}r_i} \tag{1}$$

with

$$\begin{aligned}\langle H\rangle &= \langle T\rangle + \langle V\rangle \\ &= \sum_i \frac{p_i^2}{2m_i} + \sum_i \sum_{j>i} \int f_i(\vec{r},\vec{p},t) V^{ij}(\vec{r}',\vec{r}) \\ &\quad \times f_j(\vec{r}',\vec{p}',t)\mathrm{d}\vec{r}\,\mathrm{d}\vec{r}'\,\mathrm{d}\vec{p}\,\mathrm{d}\vec{p}'.\end{aligned} \tag{2}$$

The baryon–baryon potential V^{ij} in the above relation, reads as

$$\begin{aligned}V^{ij}(\vec{r}'-\vec{r}) &= V^{ij}_{\mathrm{Skyrme}} + V^{ij}_{\mathrm{Yukawa}} + V^{ij}_{\mathrm{Coul}} + V_{\mathrm{mdi}} + V^{ij}_{\mathrm{sym}} \\ &= \left(t_1\delta(\vec{r}'-\vec{r}) + t_2\delta(\vec{r}'-\vec{r})\rho^{\gamma-1}\left(\frac{\vec{r}'+\vec{r}}{2}\right)\right) \\ &\quad + t_3\frac{\exp(|\vec{r}'-\vec{r}|/\mu)}{(|\vec{r}'-\vec{r}|/\mu)} + \frac{Z_i Z_j e^2}{|\vec{r}'-\vec{r}|} \\ &\quad + t_4 \ln^2[t_5(\vec{p}_i'-\vec{p})^2+1]\delta(\vec{r}_i'-\vec{r}) \\ &\quad + t_6\frac{1}{\varrho_0}T_3^i T_3^j \delta(\vec{r}_i{}'-\vec{r}_j).\end{aligned} \tag{3}$$

Here Z_i and Z_j denote the charges of ith and jth baryon, and T_3^i, T_3^j are their respective T_3 components (i.e. $1/2$ for protons and $-1/2$ for neutrons). The baryon potential consists of the real part of the G-matrix which is supplemented by the Coulomb interaction between the charged particles. The Coulomb potential is calculated between the pairs of interacting baryons (Z_i and Z_j) and it is not density-dependent. The parameters μ and $t_1, \ldots, t_6$ are adjusted to the real part of the nucleonic optical potential.

For the density dependence of nucleon optical potential, standard Skyrme-type parametrization is employed. The potential part resulting from the convolution of the distribution function with the Skyrme interactions V_{Skyrme} reads as

$$V_{\mathrm{Skyrme}} = \alpha\left(\frac{\rho_{\mathrm{int}}}{\rho_0}\right) + \beta\left(\frac{\rho_{\mathrm{int}}}{\rho_0}\right)^{\eta}, \tag{4}$$

where ρ_{int} is the instantaneous density and two of the three parameters of equation of state are determined by demanding that at normal nuclear matter density, the binding energy should be equal to 16 MeV. The parameters α, β and η are listed in [14,21,28].

Also, the momentum dependence of the N–N interactions $V_{\rm mdi}$, which may optionally be used in IQMD is fitted to the experimental data [30] on the real part of nucleon optical potential [31,32], which may yield

$$V_{\rm mdi} \;=\; \delta \cdot \ln^2 \left(\epsilon \cdot (\triangle p)^2 + 1\right) \cdot \left(\frac{\rho_{\rm int}}{\rho_0}\right). \tag{5}$$

The strength of symmetry energy is found to be equal to 32 MeV at normal nuclear matter density. Similarly, in the IQMD model the symmetry energy as a function of density becomes

$$E_{\rm symm}(\rho) \;=\; 32 \cdot \left(\frac{\rho_{\rm int}}{\rho_0}\right)^{\gamma}. \tag{6}$$

The term gamma (γ) determines the strength of the symmetry energy at densities away from normal nuclear matter density ($\rho_0 \;=\; 0.16\ {\rm fm}^{-3}$).

The different values of compressibility κ give rise to soft (S) and hard (H) equations of state (EOS). The compressibility factor κ is described as

$$\kappa \;=\; 9\rho^2 \frac{\partial^2}{\partial \rho^2}\left(\frac{E}{A}\right). \tag{7}$$

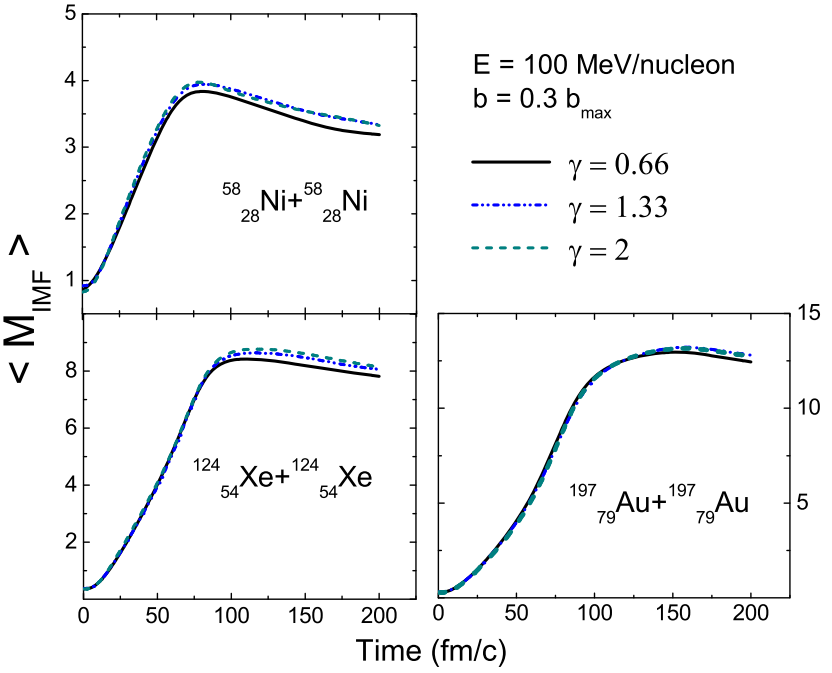

Figure 1. Time evolution of mean intermediate mass fragment (IMF) multiplicity $\langle M_{\rm IMF}\rangle$ for various systems. The incident energy is 100 MeV/nucleon and $b = 0.3 b_{\rm max}$.

For the present analysis, a soft (S) equation of state has been employed along with reduced isospin-dependent nucleon–nucleon cross-section (0.9 of σ_{NN}).

3. Results and discussion

For the present analysis, we simulated the reactions of $^{58}_{28}$Ni + $^{58}_{28}$Ni, $^{124}_{54}$Xe + $^{124}_{54}$Xe and $^{197}_{79}$Au + $^{197}_{79}$Au for few thousands of events, for the whole colliding geometry. In addition, we simulated the reactions for the systems $^{20}_{10}$Ne + $^{27}_{13}$Al, $^{40}_{18}$Ar + $^{45}_{21}$Sc, $^{84}_{36}$Kr + $^{93}_{41}$Nb, $^{129}_{54}$Xe + $^{139}_{57}$La, and $^{129}_{54}$Xe + $^{119}_{50}$Sn, at different incident energies. The phase space, thus obtained, was subjected to clusterization using minimum spanning tree MST(M) method [33] with a momentum cut of 150 MeV/c to get rid of unstable fragments. The phase space is analysed at 200 fm/c.

In figure 1, we display the time evolution of mean (intermediate mass fragment) IMF multiplicity for different forms of density-dependent symmetry energy. The very stiff form of symmetry energy, i.e. $\gamma = 2.0$, has been optimized to properly understand the impact and extent up to which the symmetry energy affects the production of intermediate mass fragments. The impact parameter of the reaction is $b = 0.3 b_{\max}$, for $b_{\max} = 1.12 (A_P^{1/3} + A_T^{1/3})$ fm, where A_P and A_T are the projectile and target mass respectively. Here, $\langle \cdots \rangle$ denotes the average over the number of events. The averaging of results over

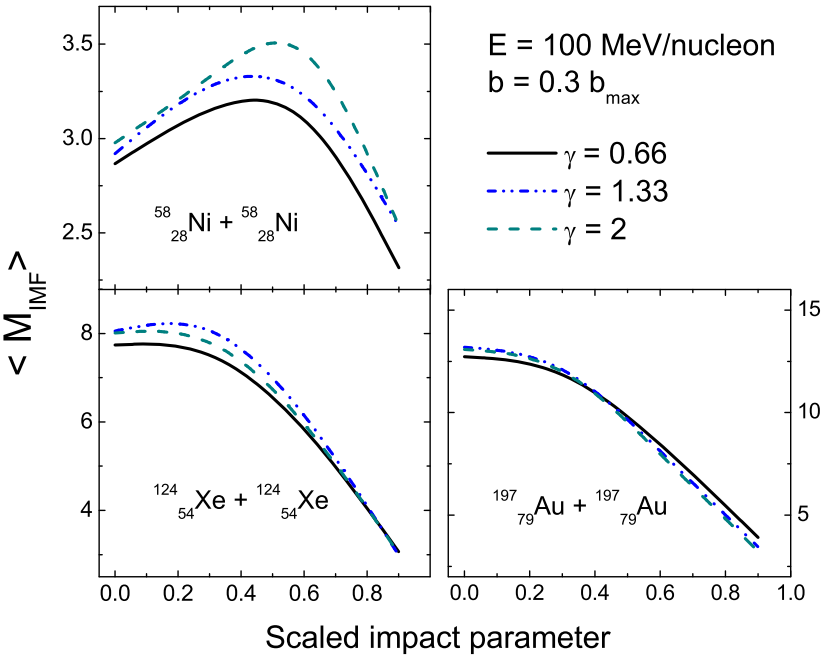

Figure 2. The impact parameter dependence of mean (intermediate mass fragment) IMF multiplicity $\langle M_{\rm IMF} \rangle$ at the incident energy of 100 MeV/nucleon.

the total number of events will nullify the statistical error and will yield a more accurate value of the observables. Though, the effect of the various forms of symmetry energy is not large, a considerable variation in the IMF production can be clearly observed. Indeed, the IMF multiplicity seems to get affected after 100 fm/c, when subjected to different forms of density-dependent symmetry energy (i.e. $\gamma = 0.66$, 1.33 and 2). This is due to the fact that the actual dissociation of the nuclear matter in a reaction starts after 100 fm/c which leads to fragmentation. The stiff forms of the symmetry energy ($\gamma = 1.33$ and 2), results in the larger IMF multiplicity as compared to $\gamma = 0.66$. Here, one could observe that for stiffer form ($\gamma = 2$), there is a drastic variation in the strength of symmetry energy but it makes only minor alteration in the yield of intermediate mass fragments.

The IMF production shows mild sensitivity towards different forms of density-dependent symmetry energy. Puri *et al* [18] stated that the fragmentation pattern of multifragmentation events in central collisions observed in the heavy-ion collisions can be recognized at a time when the particles are interacting in the highly dense system. It was concluded that the information of fragment formation can be obtained by applying simulated annealing algorithms [18]. This methodology includes the metropolis algorithm with a decreasing control parameter and is known as simulated annealing. This approach is also dubbed as simulated annealing clusterization algorithm (SACA). However, for now the fragment formation takes place when the participant matter gets saturated shortly after the decompression and the spectator/participant matter hardly interact with each other. Though SACA has the ability to detect the fragments at very early stages of the reaction,

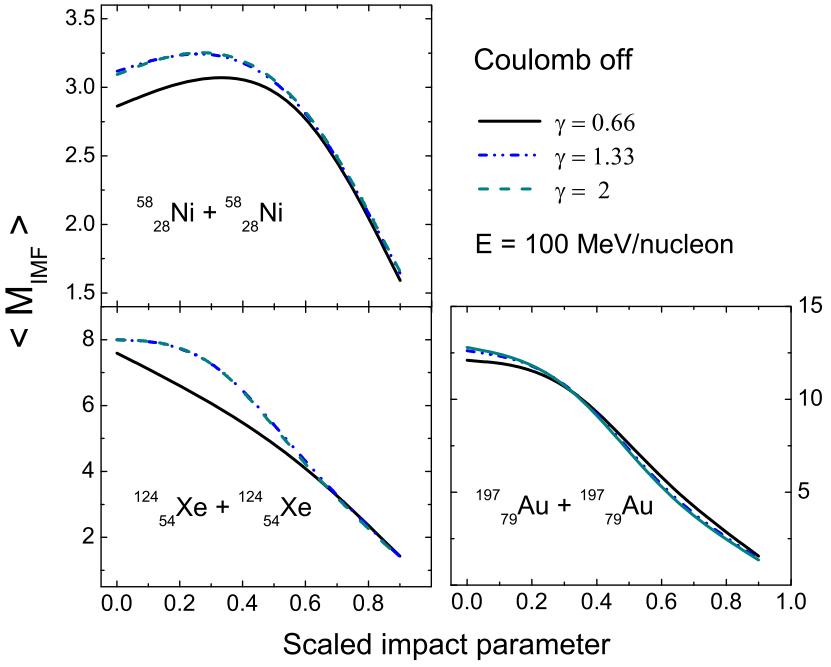

Figure 3. The impact parameter dependence of IMF multiplicity exhibiting the Coulomb interactions. The incident energy is 100 MeV/nucleon.

the MST(M) method used in the present analysis is able to detect the true reaction picture (fragment production) at 200 fm/c [33].

The impact parameter has a significant impact on the production of fragments. We display the mean IMF multiplicity for the whole colliding geometry in figure 2. One can clearly observe the larger value of $\langle M_{\mathrm{IMF}} \rangle$, for the larger value of gamma. This was also observed in figure 1. The IMF production decreases with an increase in impact parameter of the reaction. At peripheral collisions, the overlapping of target and projectile is very less, which results in the formation of heavy mass fragments. However, for the heavier systems, $^{124}_{54}$Xe + $^{124}_{54}$Xe and $^{197}_{79}$Au + $^{197}_{79}$Au, mild effect of symmetry energy is observed. The effect nearly diminishes at peripheral collisions. Interestingly, the IMF production for the $^{58}_{28}$Ni + $^{58}_{28}$Ni system, somehow shows a rise and fall behaviour, which is not observed in the other two systems. In lighter systems, the IMF-sized fragments decrease in central collisions compared to semicentral collisions. In heavier systems, the bigger size constitutes more mean field due to the larger nucleonic content and hence the IMF production is highest at central collisions. The larger influence of the mean field suppresses the production of free nucleons and light charged particles.

Coulomb effect is more dominant in heavier systems. The larger proton content in the heavier systems increases the impact of Coulomb interactions on reaction dynamics. In such a case, the Coulomb interactions overcome the symmetry energy repulsion. That is why, the IMF multiplicity is least affected in the $^{197}_{79}$Au + $^{197}_{79}$Au system. The Coulomb repulsion affects the IMF production during the dissociation (or expansion) phase. The

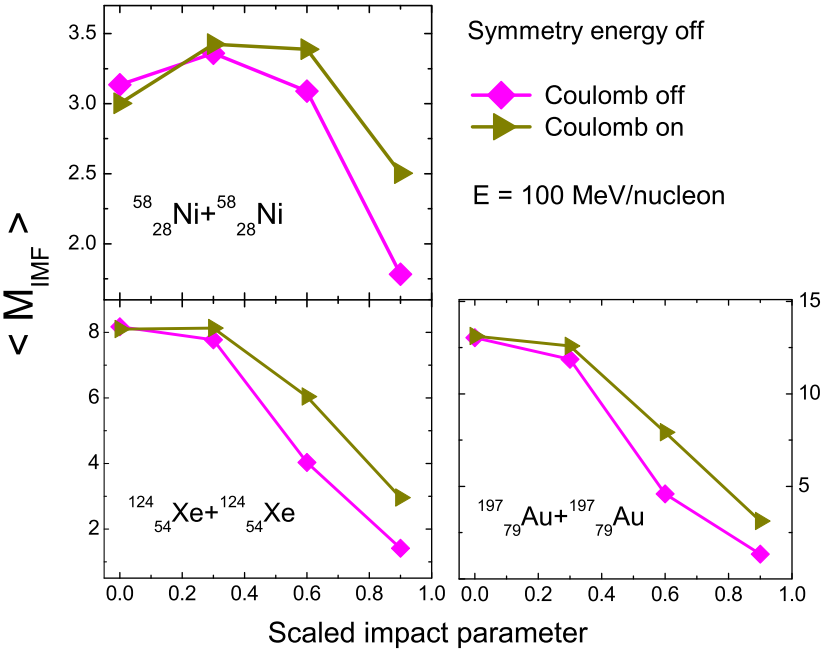

Figure 4. The impact parameter dependence of mean IMF multiplicity with the exclusion of symmetry energy. The incident energy is 100 MeV/nucleon.

Coulomb interactions have more influence on the reaction dynamics in heavier systems (systems having larger proton content). It is observed that the Coulomb interactions affect the IMF production drastically at peripheral collisions. There exists a concrete evidence that the transition energy [27] and the balance energy [1,16] decrease drastically for the heavier systems because of larger impact of Coulomb interactions in case of larger Z (protons).

To study the effect of density-dependent symmetry energy, we plot the impact parameter dependence of mean IMF multiplicity by excluding the Coulomb interactions in figure 3. We observed that in the absence of Coulomb interactions the effect of symmetry energy diminishes totally at the peripheral collisions. This is because the dissociation of nuclear matter is very less at larger impact parameters.

To understand the direct role of Coulomb interactions, we display in figure 4 the mean IMF multiplicity for the whole colliding geometry in the absence of symmetry energy. Overall, the IMF production increases with the inclusion of Coulomb interactions. This is due to the repulsion generated by the protons after the collision phase which enhance the production of IMFs due to the break-up of nuclei. One can clearly observe the larger effect of Coulomb interactions in the IMF production for peripheral collisions. This is because the violent phase of reaction in central collisions decreases the role of Coulomb interactions. A significant role of Coulomb interactions in IMF production, especially at the peripheral collisions, tends to reduce the role of various forms of symmetry energy.

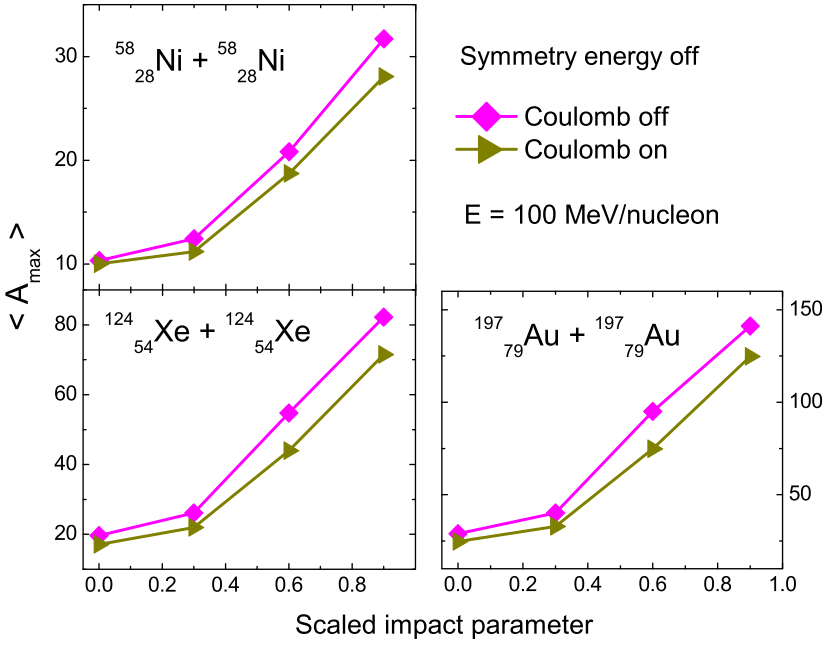

Figure 5. The variation in the mass of heaviest fragment (A_{max}) along the whole colliding geometry with the exclusion of symmetry energy. The incident energy is 100 MeV/nucleon.

In figure 5, we display the mass of the heaviest fragment ($A_{\max}$) along the whole colliding geometry with the exclusion of symmetry energy. The value of $\langle A_{\max}\rangle$ increases with the impact parameter of the reaction. This happens due to the less violent phase of the reaction at peripheral collisions. The inclusion of Coulomb interactions results in smaller value of $\langle A_{\max}\rangle$. The size of the largest fragment $\langle A_{\max}\rangle$ decreases due to the repulsion generated by the Coulomb interactions, which results in the formation of other smaller fragments (free nucleons and LMFs).

In figure 6, we display Z_{bound} along the whole colliding geometry with and without Coulomb interactions (with the exclusion of symmetry energy). The quantity Z_{bound} is defined as the sum of all atomic numbers (Z_i) of all projectile fragments with $Z_i \geq 2$. Z_{bound} is a good parameter to measure the violence of the collision and of the energy deposited in the excited spectator. Z_{bound} shows similar behaviour as that of $A_{\max}$. This reflects the disintegration of Z_{bound} with the inclusion of Coulomb interactions.

In figure 7, we display the mean multiplicity of IMFs as a function of incident energy for various systems and also compared the results with the NSCL experimental data [34]. The confrontation of the theoretical results with experimental findings can explain the complex processes which happen during nucleon–nucleon collisions. The theoretical predictions give similar trends to those of the NSCL experimental data. In $^{20}_{10}$Ne + $^{27}_{13}$Al and $^{40}_{18}$Ar + $^{45}_{21}$Sc systems the multiplicity of IMFs decreases with an increase in incident energy. For the $^{84}_{36}$Kr + $^{93}_{41}$Nb and $^{131}_{54}$Xe + $^{139}_{57}$La reactions, the mean IMF multiplicity increases with an increase in incident energy, although, in these two reactions the

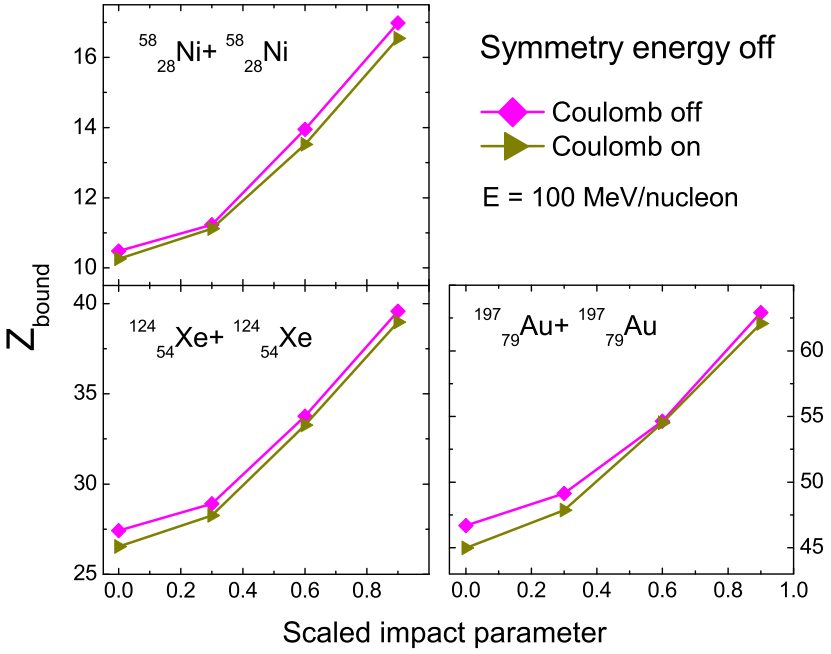

Figure 6. Z_{bound} as a function of scaled impact parameter for various systems. The incident energy is 100 MeV/nucleon.

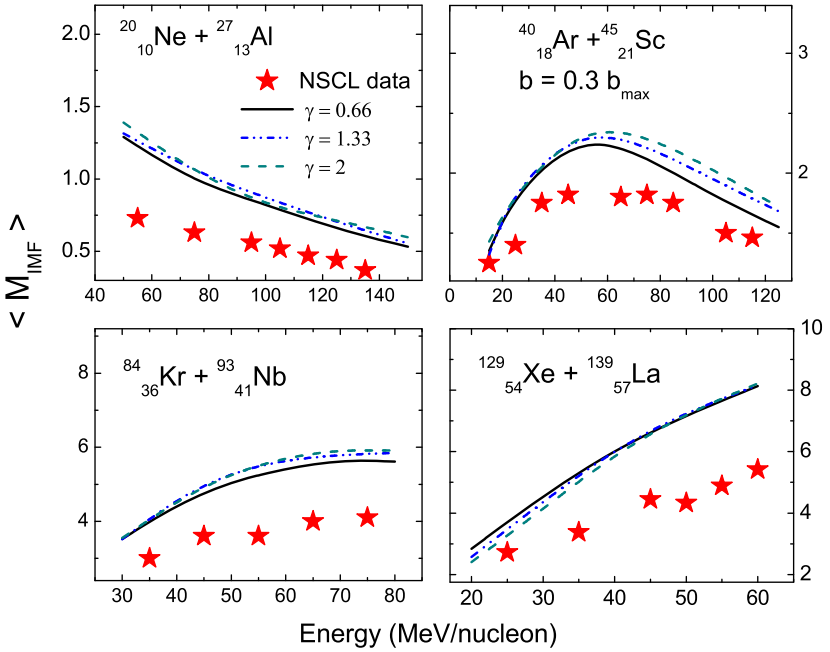

Figure 7. Mean multiplicities of IMFs as a function of incident energy and comparison with the NSCL data [34].

incident energy is much less than the first two reactions. The dynamics at low incident energies is governed by the attractive mean field. At low incident energies, of the order of 20 MeV/nucleon, we observed that the effect of symmetry energy vanishes, except for $^{131}_{54}$Xe + $^{139}_{57}$La, which can be due to the larger interplay of Coulomb interactions.

The stiffer form of symmetry energy yields lesser symmetry energy repulsion in the low-density region. That is why, the lesser neutrons are bound inside the bigger fragments in case of soft symmetry energy which decreases the IMF production. Similar findings are also observed in [35], where the neutron (proton) yield was affected by different forms of density dependence of the symmetry energy. In the $^{131}_{54}$Xe + $^{139}_{57}$La system, Coulomb interactions are more dominant affecting the reaction output. Yet the effect of density-dependent symmetry energy on the IMF production is very mild and the symmetry energy with $\gamma = 0.66$ is more compatible with the NSCL data [34] as compared to other forms ($\gamma = 1.33,\ 2$). Generally, soft density dependence of symmetry energy is recommended in the low-density region [6,35]. In [12], Shetty and Yennello observed that despite the model-dependent methodologies by which the behaviour of symmetry energy is examined, significant results have been achieved. Also, the experimental attempts and theoretical methodologies can collectively be helpful for the more accurate determination of the role of symmetry energy [12].

The theoretical predictions are based on the analysis of time-scale of fragments with spacial and momentum constraints. The experimental results imply cuts on threshold energies and angles. These cuts are very complicated in nature. The gap between the

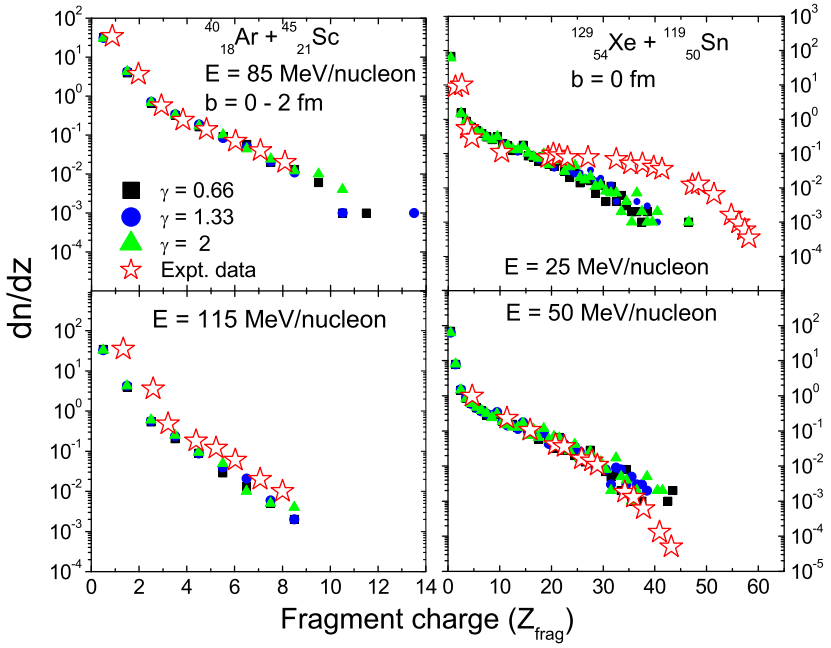

Figure 8. The charge distribution for the $^{40}_{18}\mathrm{Ar} + ^{45}_{21}\mathrm{Sc}$ reaction at the incident energies of 85 MeV/nucleon and 115 MeV/nucleon (left panels) and $^{129}_{54}\mathrm{Xe} + ^{119}_{50}\mathrm{Sn}$ at the incident energies of 25 MeV/nucleon and 50 MeV/nucleon (right panels) and a comparison with experimental data [36–40].

theoretical predictions and experimental findings is due to our inaccessibility to the filters. However, theoretical predictions yield trends similar to that of NSCL data [34].

In addition to the fragmentation, the distribution of the nuclear matter after collision can also be studied through the charge distribution corresponding to the nuclear matter. In figure 8, we display the charge distribution ($\mathrm{d}n/\mathrm{d}z$) as a function of the fragment's charge (Z_{frag}) for the $^{40}_{18}\mathrm{Ar} + ^{45}_{21}\mathrm{Sc}$ reaction (left panels) and $^{129}_{54}\mathrm{Xe} + ^{119}_{50}\mathrm{Sn}$ (right panels) and comparison with the experimental data [36–40]. The charge distribution ($\mathrm{d}n/\mathrm{d}z$) as a function of charge gives us a clear picture of the nuclear matter dissociation. A linear dependence of the charge distribution can be seen. The negative slope of the charge distribution indicates a gradual transition of the spectator matter towards total disassembly. A very mild effect of density-dependent symmetry energy on the charge distribution is observed. The increase in the incident energy corresponds to more steeper slope. For both the cases, the theoretical results are in good agreement with the experimental data [36–40].

4. Summary

In summary, the IMF production and charge distribution show a mild but considerable sensitivity towards various forms of density-dependent symmetry energy.

The small variation in IMF multiplicity is due to the fact that the phenomenon of fragmentation occurs after the collision phase when the density of the system approaches saturation density. We observed that even the very stiff form ($\gamma = 2$), does not have any impact on the production of intermediate mass fragments. Therefore, the minor sensitivity of fragment production, further strengthens our claim that the density dependence of symmetry energy (for all cases and forms) does not produce any major variation in the production of fragments during the reaction. However, the IMF multiplicity increases with the stiffness of the symmetry energy. As far as the fragment production is concerned, the effect of density-dependent symmetry energy diminishes due to the larger dominance of Coulomb interactions in the heavier systems. The inclusion of Coulomb interactions results in the disintegration of the heaviest fragment and increases the yield of intermediate mass fragments. The theoretical trends are in good agreement with the experimental data.

Acknowledgement

This work has been supported by a grant from the Department of Atomic Energy (DAE), Government of India (Grant No. 2012/37P/16/BRNS).

References

[1] A D Sood and R K Puri, *Phys. Rev. C* **69**, 054612 (2004)
[2] R K Puri and R K Gupta, *J. Phys. G* **18**, 903 (1992)
[3] P Danielewicz, R Lacey and W G Lynch, *Science* **298**, 1592 (2002)
[4] J M Lattimer and M Prakash, *Phys. Rep.* **442**, 109 (2007)
[5] B A Li, L W Chen and C M Ko, *Phys. Rep.* **464**, 113 (2008)
C Xu, B A Li and L W Chen, *Phys. Rev. C* **82**, 054607 (2010)
[6] D V Shetty, S A Yennello and G A Souliotis, *Phys. Rev. C* **76**, 024606 (2007)
[7] Y Zhang *et al*, *Phys. Lett. B* **664**, 145 (2008)
[8] M B Tsang *et al*, *Phys. Rev. Lett.* **102**, 122701 (2009)
[9] P Russotto *et al*, *Phys. Lett. B* **697**, 471 (2011)
[10] A Carbone *et al*, *Phys. Rev. C* **81**, 041301 (2010)
[11] E Khan *et al*, *Phys. Rev. C* **82**, 024322 (2010)
[12] D V Shetty and S J Yennello, *Pramana – J. Phys.* **75**, 259 (2010)
[13] C Hartnack *et al*, *Eur. Phys. J. A* **1**, 151 (1998)
[14] J Aichelin, *Phys. Rep.* **202**, 233 (1991)
[15] R K Puri *et al*, *Nucl. Phys. A* **575**, 733 (1994)
[16] A D Sood, R K Puri and J Aichelin, *Phys. Lett. B* **594**, 260 (2004)
[17] A D Sood and R K Puri, *Eur. Phys. J. A* **30**, 571 (2006)
[18] R K Puri, C Hartnack and J Aichelin, *Phys. Rev. C* **54**, R28 (1996)
[19] R K Puri and J Aichelin, *J. Comput. Phys.* **162**, 245 (2000)
[20] Y K Vermani and R K Puri, *Eur. Phys. Lett.* **85**, 62001 (2009)
[21] Y K Vermani *et al*, *J. Phys. G* **37**, 015105 (2010)
[22] C David, C Hartnack and J Aichelin, *Nucl. Phys. A* **650**, 358 (1999)
[23] C Hartnack *et al*, *Phys. Rep.* **510**, 119 (2012)
[24] S Gautam *et al*, *J. Phys. G* **37**, 085102 (2010)
[25] S Gautam, A D Sood, R K Puri and J Aichelin, *Phys. Rev. C* **83**, 034606 (2011)

[26] S Gautam, A D Sood, R K Puri and J Aichelin, *Phys. Rev. C* **83**, 014603 (2011)
[27] S Kumar, S Kumar and R K Puri, *Phys. Rev. C* **81**, 014611 (2010)
[28] E Lehmann *et al*, *Phys. Rev. C* **51**, 2113 (1995)
[29] E Lehmann *et al*, *Prog. Part. Nucl. Phys.* **30**, 219 (1993)
[30] L G Arnold and B C Clark, *Phys. Rev. C* **25**, 936 (1982)
G Passatore, *Nucl. Phys. A* **95**, 694 (1967)
[31] J Aichelin *et al*, *Phys. Rev. Lett.* **58**, 1926 (1987)
[32] G F Bertsch and S Das Gupta, *Phys. Rep.* **160**, 189 (1988)
[33] S Goyal and R K Puri, *Phys. Rev. C* **83**, 047601 (2011)
[34] W J Llope *et al*, *Phys. Rev. C* **51**, 1325 (1995)
[35] S Kumar and Y G Ma, *Phys. Rev. C* **86**, 051601(R) (2012)
[36] G D Westfall *et al*, *Nucl. Instrum. Methods A* **238**, 347 (1985)
[37] T Li *et al*, *Phys. Rev. Lett.* **70**, 1924 (1993)
[38] INDRA Collaboration: E Plagnol *et al*, *Phys. Rev. C* **61**, 014601 (1999)
[39] S Hudan, Doctorate de 1' Universite' de Caen, GANIL T **01**, 07 (2001)
[40] J D Frankland *et al*, *International Workshop on Multifragmentation and Related Topics (IWM 2001)* (LNS Catania, Italy, Nov. 28–Dec. 1, 2001)